*The AAPS Journal (2018) 20: 80*
DOI: 10.1208/s12248-018-0235-4

*Research Article*

# Assessment of Three-Drug Combination Pharmacodynamic Interactions in Pancreatic Cancer Cells

**Emilie A. G. Molins[1,2] and William J. Jusko[1,3]**

*Received 21 February 2018; accepted 20 May 2018; published online 27 June 2018*

***Abstract.*** The pharmacodynamic interactions among trifluoperazine (TFP), gemcitabine (GEM), and paclitaxel (PTX) were assessed in pancreatic cancer cells (PANC-1). The phenothiazine TFP was chosen for its potential activity on cancer stem cells, while GEM and PTX cause apoptosis. Effects of each drug alone and in various combinations on cell growth inhibition of PANC-1 cells were studied *in vitro* to determine the drug-specific parameters and assess the nature of drug interactions. Joint inhibition (JI) and competitive inhibition (CI) equations were applied with a $\psi$ interaction term. TFP fully inhibited growth of cells ($I_{max} = 1$) with an $IC_{50} = 9887$ nM. Near-maximum inhibition was achieved for GEM ($I_{max} = 0.825$) and PTX ($I_{max} = 0.844$) with an $IC_{50} = 17.4$ nM for GEM and $IC_{50} = 7.08$ nM for PTX. Estimates of an interaction term $\psi$ revealed that the combination of TFP-GEM was apparently synergistic; close to additivity, the combination TFP-PTX was antagonistic. The interaction of GEM-PTX was additive, and TFP-GEM-PTX was synergistic but close to additive. The combination of TFP $IC_{60}$–GEM $IC_{60}$–PTX $IC_{60}$ seemed optimal in producing inhibition of PANC-1 cells with an inhibitory effect of 82.1–90.2%. The addition of $\psi$ terms to traditional interaction equations allows assessment of the degree of perturbation of assumed mechanisms.

**KEY WORDS:** competitive inhibition; drug-drug interaction; joint inhibition; pancreatic cancer; pharmacodynamic interaction.

## INTRODUCTION

The standard of care of treatment for metastatic pancreatic cancer (gemcitabine and *nab*-paclitaxel) has been defined by ASCO (American Society of Clinical Oncology) (1). Gemcitabine (GEM) is a pyrimidine antimetabolite and acts in the incorporation of metabolite dFdCTP into DNA during the replication and in blocking the progression of cells at the S phase in the cell cycle leading to apoptosis. The dFdCDP also prevents the synthesis of DNA by ribonucleotide reductase (2). Paclitaxel (PTX) has been bound to albumin to improve its solubility without solvents and to decrease toxicity (3). Also, albumin enhances the transport of PTX across endothelial cells, which increases accumulation of the drug close to the tumor due to the albumin-binding protein secreted protein acidic rich in cysteine (SPARC) (3,4). The binding to albumin appears to affect the pharmacokinetics and not the pharmacodynamics; hence, PTX was chosen for these studies. PTX comes from the taxane family, is an antimicrotubule agent, and inhibits the depolymerization that leads to a stabilization of microtubules (4) causing an arrest in the G2/M phase of the cell cycle and generating apoptosis (5,6).

Trifluoperazine (TFP) was chosen for its potential activity on pancreatic cancer stem cells (CSC). It was suggested that TFP can inhibit DNA repair function and the activity of the DNA-dependent protein kinase (DNA-PK) *in vitro* (7). The phenothiazines are calmodulin antagonists and the calmodulin pathway is involved in DNA repair (7). Calmodulin is implicated in the regulation of cell proliferation, motility, and differentiation. Consequently, calmodulin antagonists decrease proliferation and also favor apoptosis via the increase of caspase 8 and Bax, reducing Bcl2, and decreasing the activation of AKT. These antagonists also enhance TRA-8-induced apoptosis of resistant pancreatic cells and prevent the recruitment of the survival signal Src (8). These effects on the apoptotic pathway were confirmed in lung cancer cells (9) and some derivatives of TFP have been patented (10).

**Electronic supplementary material** The online version of this article (https://doi.org/10.1208/s12248-018-0235-4) contains supplementary material, which is available to authorized users.

[1] Department of Pharmaceutical Sciences, School of Pharmacy and Pharmaceutical Sciences, University at Buffalo, State University of New York, Buffalo, New York 14214, USA.
[2] Ciblage Thérapeutique en Oncologie, Faculté de médecine Lyon-sud, Université Lyon 1, 69921, Oullins, France.
[3] To whom correspondence should be addressed. (e–mail: wjjusko@buffalo.edu)

Our hypothesis is that TFP combined with GEM and PTX can enhance the inhibition of proliferation by targeting cancer stem cells (CSC), one of the causes of chemotherapy resistance and relapse. In order to determine the nature and intensity of interactions (antagonism, additivity, or synergy) among the drugs, both two-drug and three-drug interactions were assessed. *In vitro* experiments utilized the pancreatic cancer cell line PANC-1. Joint inhibition (JI) and competitive inhibition (CI) equations (11–13) were used to quantify the interactions and were extended to three drugs. An interaction term $\psi$ was used to assess the degree of unexplained interaction, namely the degree of change from normal operation of the semi-mechanistic equations (14). The objective of the study is basically to determine if adding TFP to the standard of care therapeutic drugs for pancreatic cancer offers any promise towards improving efficacy in a classical *in vitro* screening cell model.

## METHODS

### Drugs

Trifluoperazine dihydrochloride was obtained from Sigma-Aldrich (St. Louis, MO). The concentration of the trifluoperazine stock solution was 50 mM in sterile Milli-Q water and stored as aliquots at 4°C. Gemcitabine hydrochloride was purchased from Sigma-Aldrich (St. Louis, MO). The concentration of the gemcitabine stock solution was 50 mM in sterile Milli-Q water and stored as aliquots at −20°C. Paclitaxel was obtained from Sequoia Research Products Ltd. (Pangbourne, UK). The concentration of the paclitaxel stock solution was 1 mM in dimethylsulfoxide (DMSO; Sigma-Aldrich) and stored as aliquots at −20°C. The highest concentration of paclitaxel led to a final concentration of 0.01% (*v*/*v*) DMSO in the culture medium.

### Cell Culture

The cell line PANC-1 was obtained from the American Type Culture Collections (Manassas, VA). Dulbecco's modified Eagle's medium (DMEM; VWR International LLC, Bridgeport, NJ) containing 10% (*v*/*v*) fetal bovine serum (FBS; VWR) was used to culture the cells. Cells were grown in a humidified atmosphere with 5% $CO_2$ at 37°C in culture flasks (Corning, Durham, NC). Each passage was done with 0.05% trypsin with 0.53 mM EDTA (Corning Inc., Corning, NY) when the confluence reached 90% of cells. The DPBS (Corning) was used to wash the cells when necessary.

### Inhibition Parameters

The experiments were performed two times for TFP, GEM, and PTX. Cells of the passages P26 and P29 were seeded in six-well plates at densities of 2.25 and $2.53 \times 10^5$ cells per well in a volume of 2 mL. A delay of 24 h allowed the cells to adhere before drug exposure. The concentrations used for each drug are listed in Table I. After drug exposure of 72 h, cells were washed with DPBS and harvested with trypsin. A Beckman Coulter Counter Z2 was used to count to cells using the isotonic diluent from Beckman Coulter (Hebron, KY). Each sample was counted in triplicate. The vehicle control was water or DMSO at the highest concentration used for the drug-treated experiments.

The experiments were carried first for two-drug interactions and then for three-drug interactions. Cells of the passage P28 were seeded in six-well plates at a density of $2.53 \times 10^5$ cells per well in a volume of 2 mL for the two-drug interactions and at a density of $2.46 \times 10^5$ for the three-drug interactions. Cells were exposed to low, medium, and high concentrations of each drug alone or in combinations. These concentrations were near the $IC_{20}$, $IC_{40}$, and $IC_{60}$ for each drug.

**Table I.** Parameter Estimates and 95% CI for Each Drug Studied Individually

| Parameters | Trifluoperazine[1] | | | Gemcitabine[2] | | | Paclitaxel[3] | | |
|---|---|---|---|---|---|---|---|---|---|
| | Value | 95% CI | CV% | Value | 95% CI | CV% | Value | 95% CI | CV% |
| *R*01 (cells) | 9.40E + 05 | – | Fix | 9.14E + 05 | (8.89–9.39)E + 05 | 1.37 | 8.78E + 05 | (8.52–9.05)E + 05 | 1.52 |
| *R*02 (cells) | 9.55E + 05 | – | Fix | 9.88E + 05 | (0.961–1.02)E + 06 | 1.37 | 9.71E + 05 | (0.941–1.00)E + 06 | 1.52 |
| $I_{max}$ | 1 | – | Fix | 0.825 | 0.815–0.835 | 0.607 | 0.844 | 0.838–0.845 | 0.353 |
| $\gamma$ | 1.84 | 1.71–1.96 | 3.37 | 2.54 | 2.33–2.76 | 4.26 | 4.34 | 4.08–4.60 | 3.02 |
| $IC_{50}$ (nM) | 9887 | 8477–11,130 | 7.13 | 17.4 | 16.8–18.0 | 1.80 | 7.08 | 6.92–7.25 | 1.17 |
| $IC_{20}$ (nM) | 4646 | 3791–5502 | 9.21 | 10.1 | 9.37–10.8 | 3.51 | 5.15 | 4.94–5.35 | 1.99 |
| $IC_{30}$ (nM) | 6232 | 5189–7275 | 8.37 | 12.5 | 11.8–13.1 | 2.74 | 5.83 | 5.64–6.02 | 1.65 |
| $IC_{40}$ (nM) | 7927 | 6705–9150 | 7.71 | 14.8 | 14.2–15.5 | 2.19 | 6.45 | 6.27–6.63 | 1.39 |
| $IC_{60}$ (nM) | 12,330 | 10,710–13,950 | 6.58 | 20.4 | 19.7–21.0 | 1.61 | 7.78 | 7.63–7.93 | 0.983 |
| $IC_{70}$ (nM) | 15,690 | 13,790–17,580 | 6.04 | 24.3 | 23.4–25.1 | 1.72 | 8.61 | 8.47–8.76 | 0.841 |
| Sigma | 0.3805 | 0.296–0.466 | 11.2 | 0.0431 | 0.0343–0.0519 | 10.2 | 0.0403 | 0.0321–0.0486 | 10.2 |
| Intercept | 0.001 | – | Fix | 0.001 | – | Fix | 0.001 | – | Fix |

[1] Concentrations used: 2251, 5437, 9456, 12,320, 16,450, 36,960, and 250,000 nM
[2] Concentrations used: 3, 8.2, 14.8, 18.5, 26.6, 57.21, and 100 nM
[3] Concentrations used: 4.257, 6.078, 7.602, 9.317, 11, 27.951, and 100 nM

### Determination of $IC_{50}$

The $IC_{50}$ of each drug was assessed as a single agent over a period of 72 h. The inhibitory form of the Hill function was used to fit the concentration-response curves.

$$R = R0_{\text{cells}} \times \left(1 - \frac{I_{\max} \times C^{\gamma}}{IC_{50}{}^{\gamma} + C^{\gamma}}\right) \quad (1)$$

with $R$, the number of per mL cells (2 mL per well); $R0_{\text{cells}}$, the baseline number of cells per mL at zero drug concentration (control); $I_{\max}$, the maximum inhibition; $IC_{50}$, the concentration that inhibits 50% of the cell growth, $\gamma$, the Hill coefficient, and $C$, the concentration of the drug. Because of different seeding numbers due to replicate experiments, the baselines were fixed to experimental values for TFP only.

The equation fittings were performed using the software ADAPT 5 (15) with the maximum likelihood method. The variance model used was as follows:

$$V = (\text{PV}(1) + \text{PV}(2) \times Y(1))2 \quad (2)$$

with $Y(1)$ the response, $PV(1)$ the intercept fixed to 0.001, and $PV(2)$ the slope.

The $IC_{20}$, $IC_{40}$, and $IC_{60}$ values were calculated from the following:

$$IC_X = \left(\frac{X}{100 - X}\right)^{1/\gamma} \times IC_{50} \quad (3)$$

with $IC_X$ the concentration inhibiting $X$% of the maximal effect.

### Interaction Analysis

For two-drug interactions, the equation for joint inhibition (JI) is as follows (11)

$$R = R0\left[1 - \frac{\left(\frac{I\max_A \times C_A^{\gamma A}}{(\psi \times IC_{50A})^{\gamma A}}\right) + \left(\frac{I\max_B \times C_B^{\gamma B}}{(IC_{50B})^{\gamma B}}\right) + (I\max_A + I\max_B - I\max_A \times I\max_B) \times \left(\frac{C_A^{\gamma A}}{(\psi \times IC_{50A})^{\gamma A}}\right) \times \left(\frac{C_B^{\gamma B}}{(IC_{50B})^{\gamma B}}\right)}{\left(\frac{C_A^{\gamma A}}{(\psi \times IC_{50A})^{\gamma A}}\right) + \left(\frac{C_B^{\gamma B}}{(IC_{50B})^{\gamma B}}\right) + \left(\frac{C_A^{\gamma A}}{(\psi \times IC_{50A})^{\gamma A}}\right) \times \left(\frac{C_B^{\gamma B}}{(IC_{50B})^{\gamma B}}\right) + 1}\right] \quad (4)$$

This is equivalent to (13):

$$R = R0 \times \left(1 - \frac{I\max_A \times C_A^{\gamma A}}{(\psi \times IC_{50A})^{\gamma A} + C_A^{\gamma A}}\right) \times \left(1 - \frac{I\max_B \times C_B^{\gamma B}}{(IC_{50B})^{\gamma B} + C_B^{\gamma B}}\right) \quad (5)$$

This equation assumed dual inhibition of a turnover process by nonspecific non-competitive mechanisms.
The traditional equation for competitive inhibition (CI) (11) is as follows:

$$R = R0\left[1 - \frac{\left(\frac{I\max_A \times C_A^{\gamma A}}{(\psi \times IC_{50A})^{\gamma A}}\right) + \left(\frac{I\max_B \times C_B^{\gamma B}}{(IC_{50B})^{\gamma B}}\right)}{1 + \left(\frac{C_A^{\gamma A}}{(\psi \times IC_{50A})^{\gamma A}}\right) + \left(\frac{C_B^{\gamma B}}{(IC_{50B})^{\gamma B}}\right)}\right] \quad (6)$$

This equation originated with Ariens et al. (12) where two drugs compete for a common target.
For three-drug interactions, the equation for JI expands to the following:

$$R = R0 \times \left(1 - \frac{I\max_A \times C_A^{\gamma A}}{(\psi \times IC_{50A})^{\gamma A} + C_A^{\gamma A}}\right) \times \left(1 - \frac{I\max_B \times C_B^{\gamma B}}{(IC_{50B})^{\gamma B} + C_B^{\gamma B}}\right) \times \left(1 - \frac{I\max_C \times C_C^{\gamma C}}{(IC_{50C})^{\gamma C} + C_C^{\gamma C}}\right) \quad (7)$$

that can also be written:

$$R = R0\left[1 - \frac{\begin{array}{c} I\max_A \times A + I\max_B \times B + I\max_C \times C + (I\max_A + I\max_B - I\max_A \times I\max_B) \times A \times B + \\ (I\max_C + I\max_B - I\max_C \times I\max_B) \times C \times B + (I\max_C + I\max_A - I\max_C \times I\max_A) \times A \times C + \\ (I\max_C + I\max_A + I\max_B - I\max_C \times I\max_A - I\max_A \times I\max_B - I\max_C \times I\max_B + I\max_C \times I\max_A \times I\max_B) \times A \times C \times B \end{array}}{A + B + C + A \times B + C \times B + A \times C + A \times B \times C + 1}\right] \quad (8)$$

with

$$A = \left(\frac{C_A^{\gamma A}}{(\psi \times \mathrm{IC}_{50A})^{\gamma A}}\right); B = \left(\frac{C_B^{\gamma B}}{(\mathrm{IC}_{50B})^{\gamma B}}\right); \quad C = \left(\frac{C_C^{\gamma C}}{(\mathrm{IC}_{50C})^{\gamma C}}\right) \tag{9}$$

The equation for the three-drug CI was as follows:

$$R = R0\left[1 - \frac{\left(\frac{I\max_A \times C_A^{\gamma A}}{(\psi \times \mathrm{IC}_{50A})^{\gamma A}}\right) + \left(\frac{I\max_B \times C_B^{\gamma B}}{(\mathrm{IC}_{50B})^{\gamma B}}\right) + \left(\frac{I\max_C \times C_C^{\gamma C}}{(\mathrm{IC}_{50C})^{\gamma C}}\right)}{1 + \left(\frac{C_A^{\gamma A}}{(\psi \times \mathrm{IC}_{50A})^{\gamma A}}\right) + \left(\frac{C_B^{\gamma B}}{(\mathrm{IC}_{50B})^{\gamma B}}\right) + \left(\frac{C_C^{\gamma C}}{(\mathrm{IC}_{50C})^{\gamma C}}\right)}\right] \tag{10}$$

with parameters having the same definitions as in Eq. 1.

The $\psi$ is the interaction term that assesses possible changes in $\mathrm{IC}_{50}$ values when data do not fit the basic equations. The interaction is apparently antagonistic if $\psi > 1$, additive if $\psi = 1$, and synergistic if $\psi < 1$.

There are different assumptions for each equation. Two drugs are said to be competitive when they share the same target. The competitive equation assumes the presence of only one target and stipulates that the maximum is equal to the maximum among single effects. Joint inhibition assumes that there are multiple targets and that the maximal effect is equal to the sum of the maximal effects of each drug (see Fig. 3 in Ref. (11)).

All equations were fitted using the software ADAPT 5 (15) with the maximum likelihood method. The variance model used was the same as Eq. 2. An example of ADAPT code and the dataset for the three-drug interactions is provided in the Supplementary Materials.

### *Methods of Modeling*

First, R0 (cells), $I_{\max}$, and $\gamma$ of each drug alone were determined specifically for the two-drug or three-drug combination experiments. Then, R0% and $\psi$ for combinations were estimated by fixing $\mathrm{IC}_{50}$, $I_{\max}$, and $\gamma$. This method assured that the intrinsic activity was considered constant to reveal interactions via the JI and CI equation structures and $\psi$ values. The $\psi$ was assigned alternatively to the $\mathrm{IC}_{50}$ of each drug to study the impact of each drug on the other.

### *Prediction Error*

To determine if one of the equations JI or CI functioned better for some interactions, the prediction error was calculated as the ratio between the predicted and true values. In our study, the true values were the data. The bias was defined as the mean of prediction errors. The inaccuracy was defined as the interquartile range of the prediction error. An interval of ± 15% was defined as acceptable. Boxplots were created with the software R.

### *Theoretical Percentages of Cells*

The theoretical percentages of cells were calculated from the data by applying the following equation for drug $A$ by using the estimates of $I\max_A$ and $\gamma A$ from the model when the drug was used as a single agent; $C_A$ and $\mathrm{IC}_{50A}$ were drug concentrations in nanomolar.

$$R_A = 100 \times \left(1 - \frac{I\max_A \times {C_A}^{\gamma A}}{{\mathrm{IC}_{50A}}^{\gamma A} + {C_A}^{\gamma A}}\right) \tag{11}$$

The same equation was applied for the second and third drugs with the new baseline equal to the number of cells found from the previous calculations (Eq. 11).

$$R_B = R_A \times \left(1 - \frac{I\max_B \times {C_B}^{\gamma B}}{{\mathrm{IC}_{50B}}^{\gamma B} + {C_B}^{\gamma B}}\right) \tag{12}$$

### *Three-Dimensional Concentration-Effect Graphs*

The interaction term $\psi$ provides a general measure of any disturbances (non-additivity) in functioning of the JI and CI equations for the combinations (16). The three-dimensional concentration-effect graphs were plotted with MATLAB for the two-drug and three-drug interactions from the final estimates of $R0$ and the previously determined values of $\mathrm{IC}_{50}$, $I_{\max}$, and $\gamma$. The colors indicated the type of interaction. For two-drug interactions, the surface represents the percentage of cells in the case of an additive interaction ($\psi = 1$). For two-drug interactions, the points provided the percentage of cells for each combination. The distance from the surface allows visualization of non-additivity.

## RESULTS

### Determination of Inhibition Parameters

The concentration-response curves of each drug alone are shown in Fig. 1. The values of the parameter estimates and their coefficients of variation (CV%) are reported in Table I. The maximum inhibition was 1.0 for TFP, 0.825 for GEM, and 0.844 for PTX. The $\mathrm{IC}_{50}$ was 9887 nM for TFP, 17.4 nM for GEM, and 7.08 nM for PTX. The $\gamma$ values were 1.84 for TFP, 2.54 for GEM, and 4.34 for PTX. As the $I_{\max}$ of TFP was equal to 1, and about 0.83 for GEM and PTX, TFP was better able to achieve full inhibition.

Table II provides parameter estimates for each drug when present in the combinations. These were different experimental runs and thus the individual drug parameters differ slightly from previous values. However, all parameters were similar to those in Table I.

### Prediction Errors

The boxplots with the prediction errors did not indicate better fittings with either of the equations: JI or CI, except for the interaction GEM-PTX that showed less variability with the JI equation and for the three-drug combination that was

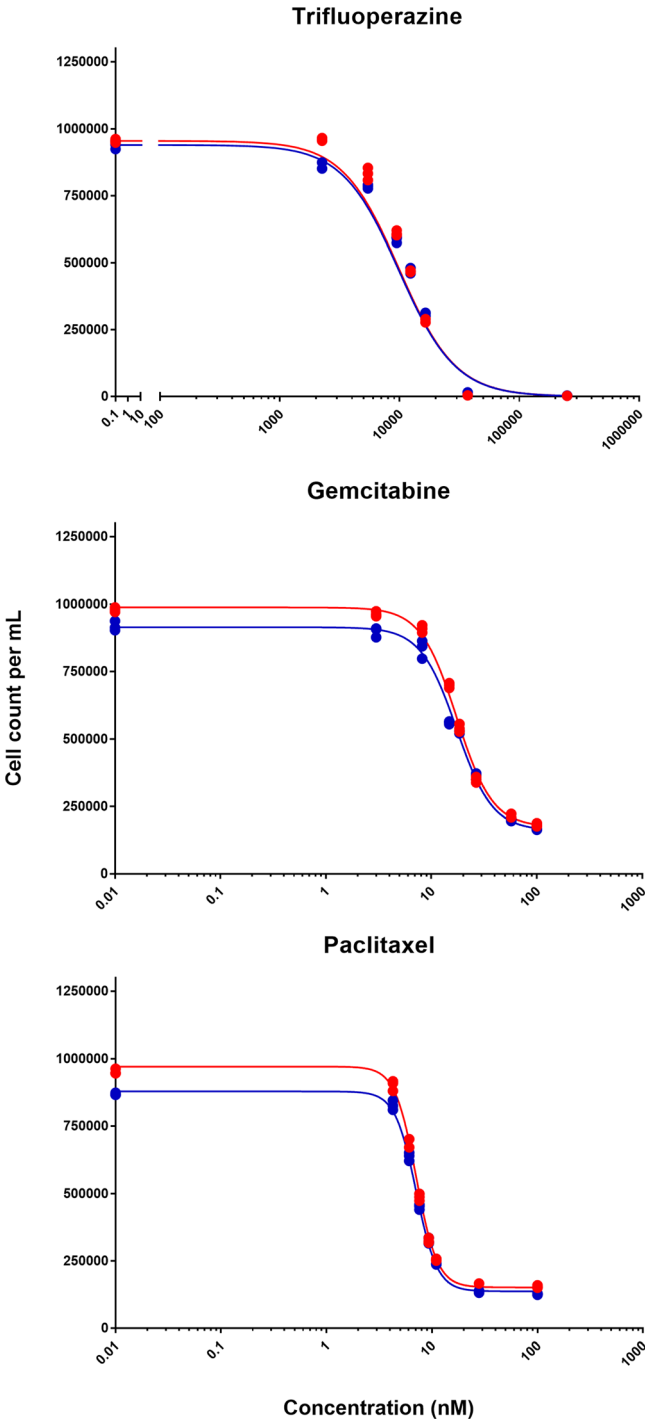


**Fig. 1.** Concentration-response curves of each indicated drug. Symbols depict data from two triplicate experiments and lines show fittings using Eq. (1)

best fitted by the CI equation. The boxplots are shown in the Supplemental Materials (Figs. S1–S4).

### Trifluoperazine-Gemcitabine Interaction

Equations 5 and 6 were used for the fittings of each pair of drugs. Figure 2 shows that as the concentration of drugs increased, the percentage of cells was reduced. The surface representing an additive interaction covered 75.5 to 26.8% cell survival, 75.5% for the combination at low concentrations and 26.8% for the high concentrations. The percentage of cells decreased more strongly with the increase of GEM concentrations than with TFP. Generally, synergy was found with some additivity for JI when the $\psi$ was applied to the GEM $IC_{50}$ at low and medium concentrations of GEM and when the $\psi$ was applied to the TFP $IC_{50}$ at low concentrations of TFP and for CI when the $\psi$ was applied to the TFP $IC_{50}$ at low concentrations of TFP and high concentration of GEM. Antagonism was found for JI when the $\psi$ was applied to the TFP $IC_{50}$ at medium and high concentrations of TFP.

To assess effects of GEM on TFP, the $\psi$ was applied to the TFP $IC_{50}$. Values of $\psi$ were 1.12 (95% confidence interval [1.10–1.13]) with slight antagonism for JI and 0.787 [0.777–0.797] with modest synergy for CI. The values are listed in Table III.

To assess effects of TFP on GEM, the $\psi$ was applied to GEM $IC_{50}$. The values were 0.969 [0.956–0.981] with slight synergy for JI and 0.866 [0.851–0.881] with synergy for CI. The values are reported in Table III.

The combination TFP $IC_{60}$-GEM $IC_{60}$, TFP $IC_{60}$-GEM $IC_{40}$ and TFP $IC_{40}$-GEM $IC_{60}$ (TFP $IC_{60}$-GEM $IC_{20}$ for $\psi$ applied to the TFP $IC_{50}$ for CI) produced the lowest number of cells. The observed percentage of cells for TFP $IC_{60}$-GEM $IC_{60}$ was around 28.5%; the predictions were 28.3% for JI and 36.0% for CI. It is important to note that the observed percentage of cells for TFP $IC_{40}$-GEM $IC_{60}$ was around 26.3%. The predicted values are reported in the heatmap (Fig. 2). This interaction was synergistic, close to additivity, because the differences between the data and the additive surface oscillated between negative and positive values as reported in Table S I. The differences between the data and the theoretical percentages of cells are displayed in the same table. They were positive, showing antagonism, but this is likely due to some variability.

### Trifluoperazine-Paclitaxel Interaction

Equations 5 and 6 were used for the fittings of each pair of drugs. Figure 3 shows that as the concentration of drugs increased, the percentage of cells was reduced. The surface representing an additive interaction covered 74.1 to 25.6% cell survival, 74.1% for the combination of both drugs at low concentrations and 25.6% at high concentrations. The percentage of cells seemed to decrease a little more with the increase of TFP concentrations than with PTX. Generally, antagonism with some additivity at TFP $IC_{40}$ and $IC_{60}$ for CI when the $\psi$ was applied to the PTX $IC_{50}$ and also for JI when the $\psi$ was applied to the TFP $IC_{50}$. Synergism was found for CI when the $\psi$ was applied to the TFP $IC_{50}$

To assess effects of PTX on TFP, the $\psi$ was applied to the TFP $IC_{50}$. The values of $\psi$ were 1.03 [1.02–1.04] for JI and 0.768 [0.761–0.775] for CI, revealing slight antagonism in the first case and modest synergy in the second. However, most of the points appeared close the surface in Fig. 3 for JI when the $\psi$ was applied to the TFP $IC_{50}$.

To assess effects of TFP on PTX, the $\psi$ was applied to the PTX $IC_{50}$. The values of $\psi$ were 1.15 [1.14–1.16] for JI and 1.02 [1.01–1.03] for CI displaying antagonism. However, most

**Table II.** Parameter Estimates for Each Drug as Single Agents for Two-Drug Combinations and Three-Drug Combination

| | | Trifluoperazine | | | Gemcitabine | | | Paclitaxel | | |
|---|---|---|---|---|---|---|---|---|---|---|
| | Parameters | Value | 95% CI | CV% | Value | 95% CI | CV% | Value | 95% CI | CV% |
| Two-drug combination | *R*0 (cells) | 1.02E + 06 | (1.01–1.03)E + 06 | 0.619 | 1.01E + 06 | (1.00–1.02)E + 06 | 0.562 | 1.01E + 06 | (0.991–1.02)E + 06 | 0.668 |
| | $I_{max}$ | 1.00 | – | Fix | 0.733 | 0.617–0.849 | 7.91 | 0.786 | 0.657–0.914 | 8.19 |
| | $\gamma$ | 1.92 | 1.81–2.03 | 2.82 | 2.57 | 2.15–3.00 | 8.32 | 3.58 | 2.83–4.32 | 10.4 |
| | $IC_{50}$ (nM) | 1.35E + 04 | (1.33–1.38)E + 04 | 0.953 | 15.8 | 13.7–17.9 | 6.71 | 6.21 | 5.60–6.83 | 4.95 |
| | Sigma | 0.0110 | 0.00653–0.0156 | 20.4 | 0.00974 | 0.00576–0.0137 | 20.4 | 0.0116 | 0.00685–0.0163 | 20.4 |
| | Intercept | 0.001 | – | Fix | 0.001 | – | Fix | 0.001 | – | Fix |
| Three-drug combination | R0 (cells) | 1.06E + 06 | (1.05–1.07)E + 06 | 0.417 | 1.03E + 06 | (1.02–1.04)E + 06 | 0.438 | 1.01E + 06 | (0.998–1.02)E + 06 | 0.580 |
| | $I_{max}$ | 1.00 | – | fix | 0.842 | 0.765–0.920 | 4.61 | 0.866 | 0.790–0.943 | 4.44 |
| | $\gamma$ | 1.87 | 1.82–1.92 | 1.35 | 2.64 | 2.37–2.91 | 5.11 | 4.51 | 3.98–5.03 | 5.81 |
| | $IC_{50}$ (nM) | 1.04E + 04 | (1.03–1.05)E + 04 | 0.580 | 15.6 | 14.4–16.8 | 3.82 | 6.40 | 6.12–6.68 | 2.19 |
| | Sigma | 0.00734 | 0.00421–0.0105 | 21.3 | 0.00758 | 0.00449–0.0107 | 20.4 | 0.0101 | 0.00595–0.0142 | 20.4 |
| | Intercept | 0.001 | – | Fix | 0.001 | – | Fix | 0.001 | – | Fix |

of the data were close the surface in Fig. 3 for CI when the $\psi$ was applied to the PTX $IC_{50}$. The values are presented in Table III.

The combination TFP $IC_{60}$-PTX $IC_{60}$, TFP $IC_{60}$-PTX $IC_{40}$, and TFP $IC_{40}$-PTX $IC_{60}$ (or TFP $IC_{60}$-PTX $IC_{20}$ for CI when the $\psi$ was applied to the TFP $IC_{50}$), produced the lowest number of cells. The observed percentage of cells for TFP $IC_{60}$-PTX $IC_{60}$ was around 28.4%; the predictions were 29.1% for JI and 36.6% for CI. The values are reported in the heatmap (Fig. 3). This interaction was antagonistic, close to additive, because the differences between the data and the additive surface were generally positive, as reported in

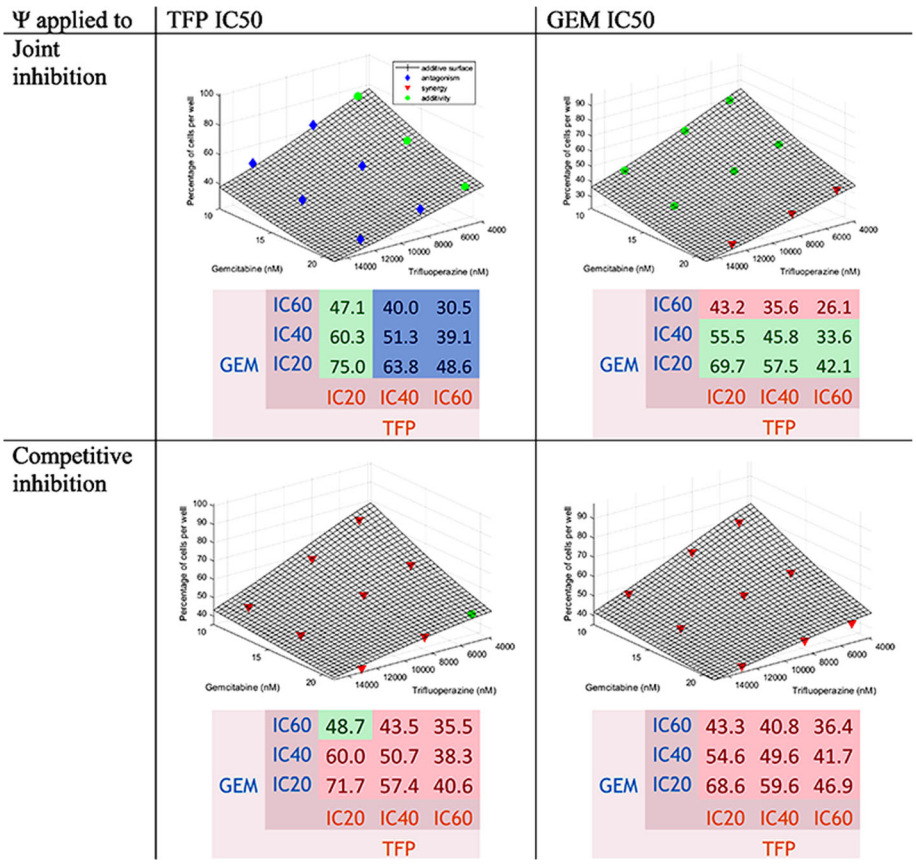


**Fig. 2.** Concentration-effect graph and predicted percentage of cells for the interaction TFP-GEM for joint inhibition and competitive inhibition with $\psi$ applied to TFP and GEM $IC_{50}$ values. The surface represents the additive interaction. The points in blue are above the surface (antagonism); in green, if within 2.5% of the additive surface; and in red, when below the surface (synergy)

**Table III.** Parameter Estimates for the Two-Drug Combinations

| | | | *Ψ for TFP* | | | *Ψ for GEM* | | |
|---|---|---|---|---|---|---|---|---|
| | | | Estimates | 95% CI | CV (%) | Estimates | 95% CI | CV (%) |
| Interaction of trifluoperazine and gemcitabine | | R0 (%) | 101 | 101–102 | 0.272 | 97.7 | 96.9–98.5 | 0.394 |
| | *Joint inhibition* | *Ψ* | 1.12 | 1.10–1.13 | 0.570 | 0.969 | 0.956–0.981 | 0.647 |
| | | Sigma | 0.00994 | 0.00737–0.0125 | 12.9 | 0.0115 | 0.00849–0.0144 | 12.9 |
| | | Intercept | 0.001 | – | Fix | 0.001 | – | Fix |
| | *Competitive inhibition* | *Ψ* | 0.787 | 0.777–0.797 | 0.647 | 0.866 | 0.851–0.881 | 0.865 |
| | | Sigma | 0.0142 | 0.0106–0.0179 | 12.9 | 0.0134 | 0.00989–0.0168 | 12.9 |
| | | Intercept | 0.001 | – | Fix | 0.001 | – | Fix |
| | | | *Ψ for TFP* | | | *Ψ for PTX* | | |
| | | | Estimates | 95% CI | CV (%) | Estimates | 95% CI | CV (%) |
| Interaction of trifluoperazine and paclitaxel | | *R*0 (%) | 110 | 110–111 | 0.203 | 105 | 105–106 | 0.311 |
| | *Joint inhibition* | *Ψ* | 1.03 | 1.02–1.04 | 0.390 | 1.15 | 1.14–1.16 | 0.342 |
| | | Sigma | 0.00758 | 0.00558–0.00957 | 13.2 | 0.00822 | 0.00605–0.0104 | 13.2 |
| | | Intercept | 0.001 | – | Fix | 0.001 | – | Fix |
| | *Competitive inhibition* | *Ψ* | 0.768 | 0.761–0.775 | 0.455 | 1.02 | 1.01–1.03 | 0.412 |
| | | Sigma | 0.00863 | 0.00636–0.0109 | 13.2 | 0.00962 | 0.00709–0.01215 | 13.2 |
| | | Intercept | 0.001 | – | Fix | 0.001 | – | Fix |
| | | | *Ψ for GEM* | | | *Ψ for PTX* | | |
| | | | Estimates | 95% CI | CV (%) | Estimates | 95% CI | CV (%) |
| Interaction of gemcitabine and paclitaxel | | *R*0 (%) | 97.0 | 94.2–99.9 | 1.45 | 98.2 | 94.6–102 | 1.80 |
| | *Joint inhibition* | *Ψ* | 1.05 | 0.997–1.10 | 2.36 | 1.02 | 0.981–1.05 | 1.69 |
| | | Sigma | 0.0337 | 0.0250–0.0424 | 12.9 | 0.0372 | 0.0275–0.0468 | 12.9 |
| | | Intercept | 0.001 | – | Fix | 0.001 | – | Fix |
| | *Competitive inhibition* | *Ψ* | 0.640 | 0.559–0.721 | 6.32 | 0.794 | 0.741–0.846 | 3.31 |
| | | Sigma | 0.128 | 0.09434–0.161 | 13.1 | 0.125 | 0.0921–0.157 | 13.1 |
| | | Intercept | 0.001 | – | Fix | 0.001 | – | Fix |

Table S II. The differences between the data and the theoretical percentages of cells are displayed in the same table. They were positive, showing antagonism.

### Gemcitabine-Paclitaxel Interaction

Equations 5 and 6 were used for the fittings of each pair of drugs. Figure 4 shows that as the concentration of drugs increased, the percentage of cells was reduced. The surface representing an additive interaction covered 64.0 to 22.8% cell survival, 64.0% for the combination at low concentrations and 22.8% for the high concentrations. The percentage of cells decreased more strongly with PTX than with GEM. Generally, additivity, close to synergism, was found. Additivity was found for JI when the $\psi$ was applied to the PTX $IC_{50}$ and at low concentration of GEM when the $\psi$ was applied to the GEM $IC_{50}$. Antagonism with JI when the $\psi$ was applied to the GEM $IC_{50}$ was found at medium and high concentrations of GEM. Synergy was found with CI.

To assess the effect of PTX on GEM, the $\psi$ was applied to the GEM $IC_{50}$. The values of $\psi$ were 1.05 [0.997–1.10] showing additivity for JI and 0.640 [0.559–0.721] with synergism for CI.

To assess the effect of GEM on PTX, the $\psi$ was applied to the PTX $IC_{50}$. The values of $\psi$ were 1.02 [0.981–1.05] showing additivity for JI and 0.794 [0.741–0.846] with slight synergism for CI. The values are displayed in Table III.

The combinations GEM $IC_{60}$-PTX $IC_{60}$, GEM $IC_{60}$-PTX $IC_{40}$, and GEM $IC_{40}$-PTX $IC_{60}$ were the ones producing the lowest number of cells for JI. The combinations GEM $IC_{60}$-PTX $IC_{60}$, GEM $IC_{60}$-PTX $IC_{40}$, and GEM $IC_{60}$-PTX $IC_{20}$ produced the lowest number of cells for CI when the $\psi$ was applied to the GEM $IC_{50}$. The combinations GEM $IC_{60}$-PTX $IC_{60}$, GEM $IC_{40}$-PTX $IC_{60}$, and GEM $IC_{20}$-PTX $IC_{60}$ produced the lowest number of cells for CI when the $\psi$ was applied to the PTX $IC_{50}$.

The observed percentage of cells for GEM $IC_{60}$-PTX $IC_{60}$ was 24.0%; the predictions were around 23.6% for JI and 32.0% for CI. The values are reported in the heatmap (Fig. 4). This interaction was additive, because the differences between the data and additive surface were below zero with some positive values as reported in Table S III. The differences between the data and the theoretical percentages of cells are displayed in the same table. They were generally negative; thus, the interaction was probably slightly synergistic, close to additive.

### Trifluoperazine-Gemcitabine-Paclitaxel Interaction

Equations 7 and 10 were used for the fittings. Figure 5 shows that for JI, there is antagonism, and for CI, there is synergism.

To assess the effect of GEM and PTX on TFP, the $\psi$ was applied to the TFP $IC_{50}$. The values of $\psi$ were 1.20 [1.15–1.25] showing antagonism for JI and 0.559 [0.539–0.579] with synergism for CI.

To assess the effect of TFP and PTX on GEM, the $\psi$ was applied to the GEM $IC_{50}$. The values of $\psi$ were 1.60 [1.57–1.63] revealing antagonism for JI and 0.507 [0.498–0.515] with synergism for CI.

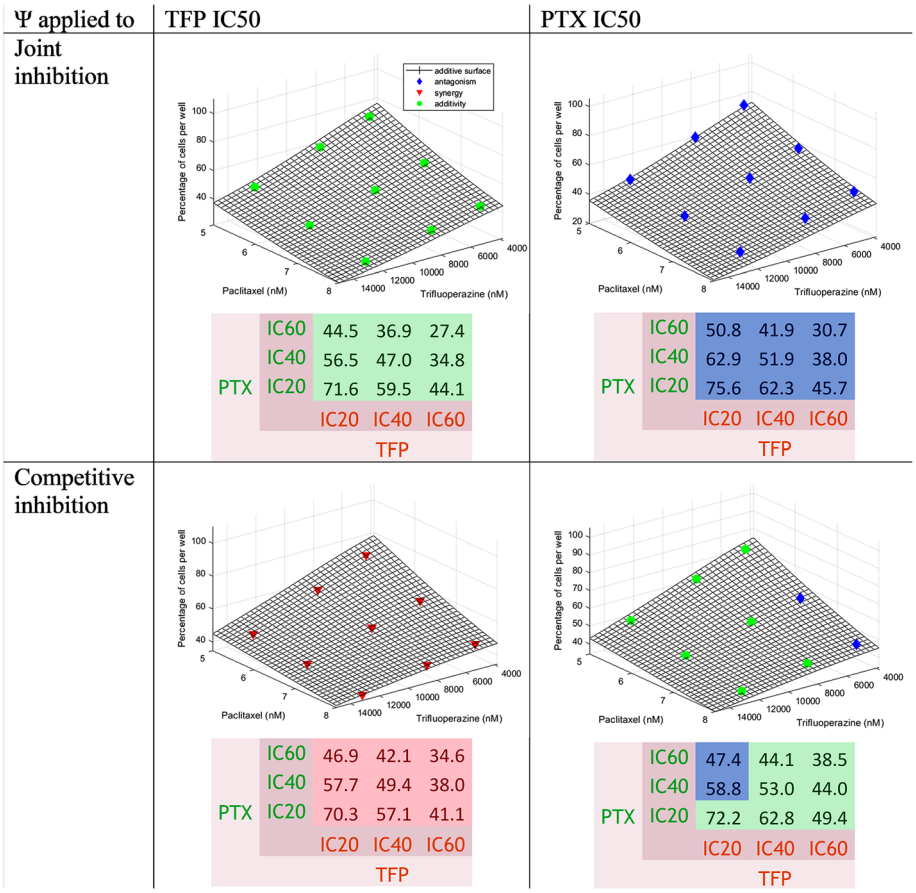


**Fig. 3.** Concentration-effect graph and predicted percentage of cells for the interaction TFP-PTX for joint inhibition and competitive inhibition with $\psi$ applied to TFP and PTX $IC_{50}$ values. The surface represents the additive interaction. Colors are defined in Fig. 2

To assess the effect of TFP and GEM on PTX, the $\psi$ was applied to the PTX $IC_{50}$. The values of $\psi$ were 1.23 [1.20–1.27] demonstrating antagonism for JI and 0.704 [0.686–0.723] with synergy for CI. The values are described in Table IV.

Not surprisingly, the combination TFP $IC_{60}$-GEM $IC_{60}$-PTX $IC_{60}$ produced the lowest number of cells. The observed percentage of cells for TFP $IC_{60}$-GEM $IC_{60}$-PTX $IC_{60}$ was 17.6% and the predictions were 9.83% for JI and 17.9% for CI. The values were reported in the heatmap (Fig. 6).

This interaction was antagonistic using JI and synergistic with CI because the differences in percentages of cells between the data and the additive surface were usually above 0 with JI and slightly negative for CI, as reported in Table S IV. In the same table, the differences between the data and the theoretical percentages of cells are displayed and oscillated between negative and positive values, generally displaying additivity. At the high concentrations of drugs, the differences were greater displaying more antagonism when high concentrations of one or several drugs were used.

## DISCUSSION

### Cell Lines and Combination Index Formulas

The cell line PANC-1 was used because this cell line has the highest proportion (7.57%) of side population cells compared to other pancreatic cancer cells: BxPc-3 (0.79%), CFPAC-1 (2.59%), MIA PaCa-2 (0.03%), and SW1990 (4.19%). The side population cells have the same characteristic of CSC (17).

### Determination of $IC_{50}$

The TFP $IC_{50}$ was 9887 nM, i.e., 9.887 μM. In non-small cell lung cancer cell lines, the TFP $IC_{50}$ was in the range 7.2 to 15 μM (see Table 2 in (9)). The $IC_{50}$ was 6 μM in P388 murine leukemic cells and in their multidrug-resistant clone (18). Our value agrees with these literature results. However, peak plasma concentrations found in humans were about 3 μg/L for a dose of 5 mg of TFP (19). The 9887 nM corresponds to 4750 μg/L, i.e., more than one thousand times higher. Based on the affinity constant between TFP and albumin ($K_{Alb} = 3.3 \times 10^4\ M^{-1}$ (20)) and alpha-1-acid glycoprotein ($K_{\alpha 1gp} = 6.0 \times 10^5\ M^{-1}$ (20)), the calculated fraction unbound is 2.80% in humans, leading to a TFP-free concentration of 0.0866 μg/L. Concentrations of 4.3 g/dL of albumin (MW of 65,000 Da) and 0.9 g/L for alpha-1-acid glycoprotein (MW of 42,000 Da) and one binding site for TFP was assumed for each protein.

*In vitro*, FBS contains 2.1 g/dL of albumin and 0.10 g/dL of alpha-1-acid glycoprotein. As 50 mL of FBS were added to the DMEM, these protein concentrations in the final DMEM were 1.91 and 0.09 g/L, leading to a calculated fraction unbound of 42.9% for a concentration of free TFP of 2036 μg/L.

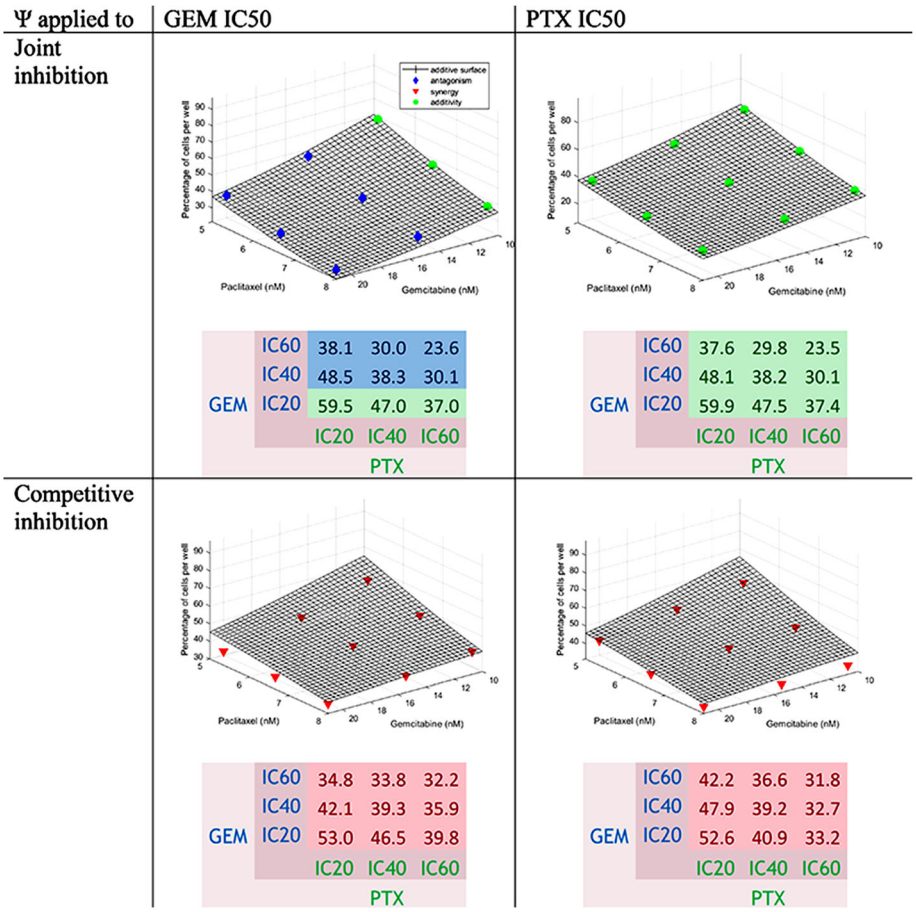


**Fig. 4.** Concentration-effect graph and predicted percentage of cells for the interaction GEM-PTX for joint inhibition and competitive inhibition with $\psi$ applied to GEM and PTX $IC_{50}$ values. The surface represents the additive interaction. Colors are defined in Fig. 2

While such high TFP concentrations are not feasible for patients, mouse studies with xenografts were conducted at a dose of 5 mg/kg/day equivalent to a human dose of 28 mg/day. The authors observed a smaller tumor size compared to the control and gefitinib, and also a sensitization to gefitinib-resistant lung cancer cells (9). While the comparison of TFP concentrations *in vitro* and *in vivo* is complex, these differences in doses offer a pharmacologic feasibility perspective. If TFP acts primarily on CSC with its own renewal and differentiation and must distribute into a tumor, then $IC_{50}$ cannot be directly scaled.

The GEM $IC_{50}$ was 17.4 nM. This is consistent with previous values for the same cell line (PANC-1), which was 20 nM for a basic PD model and 6 nM for a mechanism-based model (21). Another study found an $IC_{50}$ of 17.9 nM for the PANC-1 cells (22). The $C_{max}$ of gemcitabine was about 30 μM in lung cancer patients after a dose of 1000 mg/m$^2$ (23) or 24,500 μg/L (24), much higher than our $IC_{50}$ of 17.4 nM, i.e., 5.21 μg/L. According to the FDA, the plasma protein binding is negligible (25), probably around 10% (26).

The PTX $IC_{50}$ for eight human cancer cell lines ranged between 2.5 and 7.5 nM (27). This is close to our result of 7.08 nM. The $C_{max}$ of paclitaxel was 3.2 μM in lung cancer patients after a dose of 150 mg/m$^2$ (23) or 7916 μg/L after a dose of 125 mg/m$^2$ (28), much higher than our $IC_{50}$ of 7.08 nM, i.e., 6.05 μg/L. According to the FDA, 89 to 98% of paclitaxel was bound from in vitro studies of binding to human serum proteins (29).

The estimates found for the drugs as single agents for two-drug and three-drug combinations, based on their $IC_{20}$, $IC_{40}$, and $IC_{60}$ values, were similar to what was found with the concentration-response curves. Thus, these values were fixed during the fitting of JI and CI equations to assure that any interaction will be revealed from the model and $\psi$ values.

## Theoretical Percentages of Cells

The method using Eqs. (11) and (12) to calculate the theoretical percentages of cells can be used to assess the percentages of cells in the case of additive interactions. This method has the advantage of using only information from the fittings of the single agents.

## Two-Drug Interactions

The confidence intervals of $\psi$ were probably narrow due to the fact that the single-drug effects were very well captured with the Hill-type equations and were fixed afterwards; the baseline is close to 100%, leaving the $\psi$ values very well estimated.

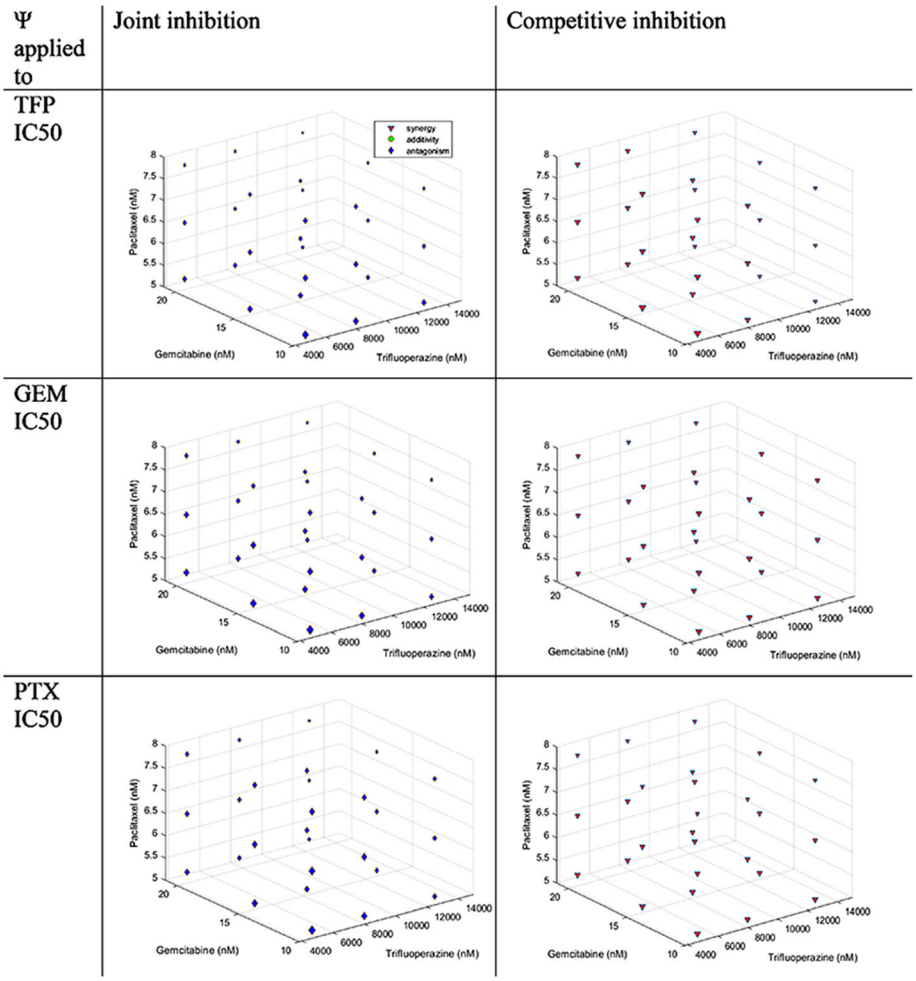


**Fig. 5.** Concentration-effect graph for the interaction TFP-GEM-PTX for joint inhibition and competitive inhibition with $\psi$ applied to TFP, GEM, and PTX $IC_{50}$ values. Colors are defined in Fig. 2

*Trifluoperazine-Gemcitabine Interaction*

In most cases, the combinations of TFP and GEM were synergistic, close to additive, according to the 3-D graphs. The use of JI and CI mechanisms led generally to the same conclusion. Moreover, TFP seemed to make GEM slightly more potent, as the $\psi$ was below 1 (synergy) when it was applied to the GEM $IC_{50}$. The effect of GEM on TFP seemed more additive.

The possible anti-apoptotic activity or the effect of TFP on CSC combined with the effect of GEM can explain the observed additivity. In a study on lung cancer cells, TFP induced increases in Bax, Bak, cleaved PARP, and caspases 3 and 9 and reductions in Bcl2, XIAP, and Mcl-1. Moreover, an effect on CSC was reported (9). The CSC subpopulation of cells features more infiltration, greater plasticity, high differentiation capacity, and self-renewal potential. This leads to an

**Table IV.** Parameter Estimates for the Interaction of Trifluoperazine and Gemcitabine and Paclitaxel

| | | $\Psi$ for TFP | | | $\Psi$ for GEM | | | $\Psi$ for PTX | | |
|---|---|---|---|---|---|---|---|---|---|---|
| | | Estimates | 95% CI | CV (%) | Estimates | 95% CI | CV (%) | Estimates | 95% CI | CV (%) |
| Joint inhibition | *R*0 (%) | 100 | 97.7–102 | 1.13 | 100 | 99.2–101 | 0.388 | 100 | 97.3–103 | 1.35 |
| | $\Psi$ | 1.20 | 1.15–1.25 | 1.95 | 1.60 | 1.57–1.63 | 0.872 | 1.23 | 1.20–1.27 | 1.32 |
| | Sigma | 0.0699 | 0.0594–0.0805 | 7.53 | 0.0257 | 0.0219–0.0296 | 7.51 | 0.0893 | 0.0758–0.103 | 7.55 |
| | Intercept | 0.001 | – | Fix | 0.001 | – | Fix | 0.001 | – | Fix |
| Competitive inhibition | $\Psi$ | 0.559 | 0.539–0.579 | 1.81 | 0.507 | 0.498–0.515 | 0.825 | 0.704 | 0.686–0.723 | 1.34 |
| | Sigma | 0.0865 | 0.0735–0.0996 | 7.55 | 0.0231 | 0.0196–0.0266 | 7.51 | 0.0703 | 0.0597–0.0809 | 7.53 |
| | Intercept | 0.001 | – | Fix | 0.001 | – | Fix | 0.001 | – | Fix |

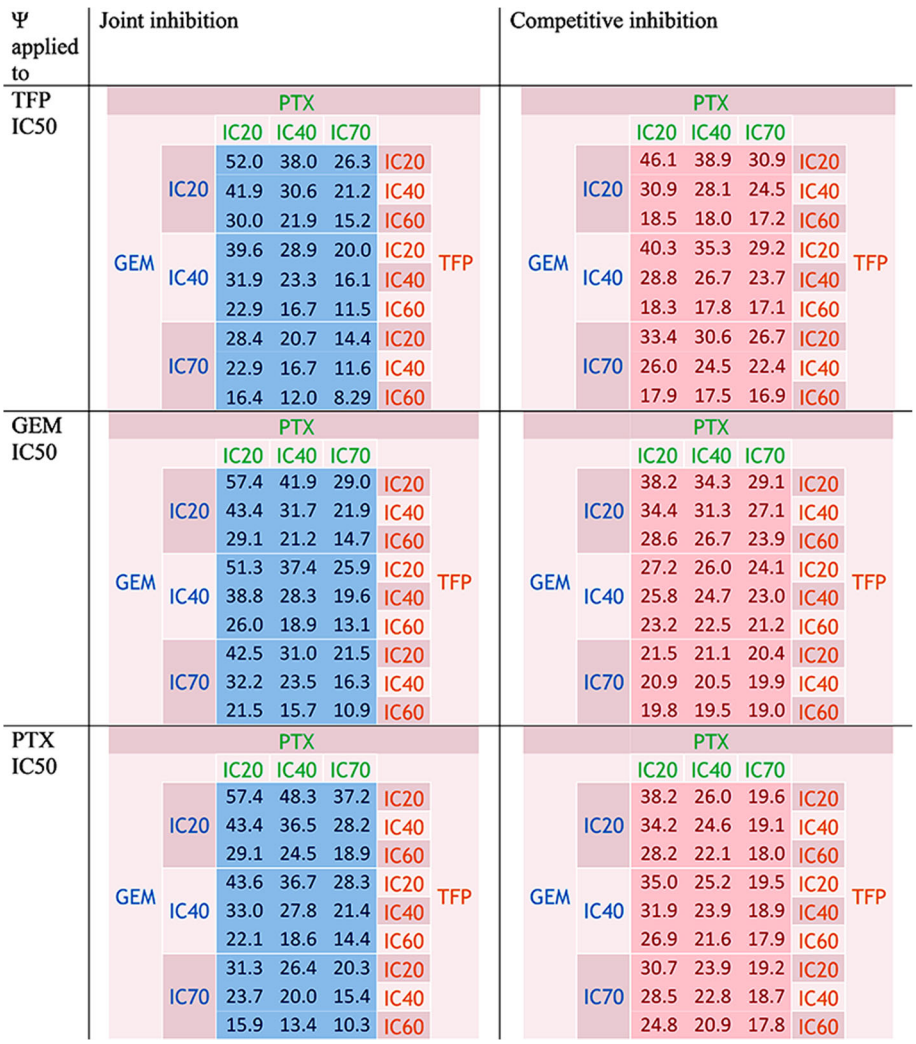


**Fig. 6.** Predicted percentage of cells for the interaction TFP-GEM-PTX for joint inhibition and competitive inhibition with $\psi$ applied to TFP, GEM, and PTX $IC_{50}$ values. Colors are defined in Fig. 2

intratumoral heterogeneity and high tumorigenicity causing resistance to chemotherapy, recurrence, and clinical relapse (30–32). One clinical study evaluated the rate of recurrence during chemotherapy as 37%. The overall survival of patients without recurrence was estimated at 26.3 *versus* 9.3 months for patients with relapse ($P < 0.001$) (33). The authors observed a reduction of the number and volume of CSC tumor spheroids, a decline in CSC markers, especially CD44 and CD133, and a decrease in the $ALDH^+$ subpopulation of CSC. Moreover, TFP decreased the targets of the Wnt/β-catenin pathway: cyclin D1, c-Myc, and c-Met (9). The $CD133^+$ cells were involved in chemoresistance (31). According to different studies, $ALDH^{high}$ cells were associated with a poor overall survival and are tumorigenic (31,34–36). Moreover, $CD44^+$ $c\text{-}Met^{high}$ were described as highly metastatic (31) and $c\text{-}Met^{high}$ had a capacity of self-renewal and a tumorigenic potential (35). CD44 as well as Epcam are involved in the Notch signaling pathway (35,36). CD44 as well as CD24 and Epcam are part of the sonic Hedghog pathway (31,35,37) and CD133 is part of the PI3K/AKT/mTOR pathway (35,36).

Because JI and CI results appeared similar in the boxplots (Supplemental Fig. S1), it was difficult to assess if the apparent synergy comes from the fact that they act on the same target (CI), i.e., due to the apoptotic effect of TFP or if they act on different targets (JI), in which case it is not possible to determine if the synergy was due to a direct anti-apoptotic effect or via anti-CSC effects of TFP.

Conatumumab and tigatuzumab targeting DR5 and cabozantinib targeting c-Met were or are currently in clinical trials for pancreatic cancer and seem to act on the $ALDH^+$ and $CD44^+CD24^+$ cell populations for tigatuzumab and on $c\text{-}Met^{high}CD44^+$ and $CD44^+CD24^+ESA^+$ for cabozantinib (38,39). Cabozantinib was approved for renal and thyroid carcinomas. Conatumumab was abandoned but several studies are running for tigatuzumab. Thus, TFP seemed a good candidate to evaluate.

### *Trifluoperazine-Paclitaxel Interaction*

As most of the $\psi$ values were above but close to 1, the interaction TFP-PTX was antagonistic, close to additive. The

use of JI and CI mechanisms led roughly to the same conclusion. Moreover, the effect of PTX on TFP seemed additive, and the effect of TFP on PTX appears antagonistic, because $\psi$ was above 1.

*Gemcitabine-Paclitaxel Interaction*

The interaction GEM-PTX was additive, close to synergy. The equations do not lead to the same conclusions. The interactions were additive for JI. The interactions were synergistic for CI. The boxplots in Fig. S3 seemed less variable with JI; thus, the interaction was probably additive.

The combination GEM-PTX has been well studied. Additivity was found when the drugs were used simultaneously and when GEM was followed by PTX. The same study showed a synergistic effect on the growth inhibition of a breast cancer cell line if PTX was used during the first 24 h and GEM in the following 48 h. The range of concentrations was 0.1–29.3 nM for PTX and 3.34–3337 nM for GEM (5). These were similar to our concentrations. Likewise, in a combination study of GEM-PTX in non-small-cell lung cancer cells, more apoptotic cells were observed when PTX was given prior to GEM. A possible explanation can be the increase of dFdCTP (active form of GEM) and its increased incorporation into RNA. Deoxycytidine kinase levels and incorporation into DNA were not affected by PTX (40). Despite these positive effects, all the interactions were additive or antagonistic, as the range of combination index values was 1–2.6. The range of $IC_{50}$ values was 5.6–88 nM for PTX and 4.3-25 nM for GEM, which were similar to our study. This was confirmed by the results from a clinical trial in non-small-cell lung cancer (NSCLC) patients. They found no pharmacokinetic interaction, but showed an increase in dFdCTP accumulation which improved the antitumor activity (23). This increase would be the consequence of the inhibition by PTX of cytidine deaminase, the enzyme responsible of the production of the inactive metabolites: dFdU, leading to an increase in the ratio dFdC/dFdU and an increase of dFdCTP in tumors. This inhibition is a PTX-induced ROS mechanism and can be overturned by N-acetylcysteine (41). The metabolic pathway of GEM is presented in Fig. S5.

However, other studies by the same authors reached different conclusions. Synergy was demonstrated between GEM-PTX in the same type of cancer (non-small-cell lung cancer cells) and PTX caused an increase in deoxycytidine kinase and cytidine deaminase activity despite a decrease in their mRNA and PTX decreased deoxycytidine kinase protein but did not affect cytidine deaminase protein (42), leading to a decrease in dFdU, but PTX did not affect significantly the intracellular accumulation of the triphosphate metabolite. The authors reported that above 20 μM of GEM a saturation of deoxycytidine kinase occurred (43) and also that PTX decreased the systemic clearance and volume of distribution of GEM (44).

Antagonism between these two drugs was found in a study where GEM and PTX were used simultaneously or sequentially in human lung A549, breast MCF7, and pancreas adenocarcinoma P-SW cell lines. The authors concluded that GEM antagonized the cell killing from PTX. At that time, they also urged caution for the clinical trials combining both drugs (45). Nevertheless, the combination GEM and *nab*-PTX extended patient survival. The protocol used in common practice is administration of 125 mg/m$^2$ of *nab*-paclitaxel followed by 1000 mg/m$^2$ of gemcitabine IV over 30–40 min on days 1, 8, and 15 of each 28-day cycle (46,47).

There are other possible reasons of the success of the combination GEM-PTX, beyond the increase in the active metabolite dFdCTP. Fragmentation of DNA was found with this drug combination in one study (5). It was possible that GEM and PTX acted on the same pathway among the Bax/Bcl2 apoptotic pathway and especially the Bcl-2-related mitochondrial apoptotic pathway, but perhaps on different targets since JI seemed better. In the treatment schedule where PTX was followed by GEM, there was an increase of the ratio Bax/Bcl2 (Bax is pro-apototic and Bcl2 is anti-apoptotic) (5). A potential reason for the additivity observed *in vitro*, but of the good efficacy *in vivo* of the combination GEM-PTX, may be the inhibitory effect of PTX on the pancreatic stellate cells (PSC), demonstrated in a model using a 3D culture (48).

At a ratio of 10/1, GEM/PTX was found synergistic in PANC-1 cells (combination index = 0.5). These values correspond to 8343 nM of GEM and 293 nM of PTX. It is important to note that the $IC_{50}$ found with PANC-1 cells by the authors (GEM $IC_{50}$ = 60,736 nM, PTX $IC_{50}$ = 9369 nM) were much higher than our values (49).

## Three-Drug Interactions

The interaction equations do not consistently lead to the same conclusions. The interaction TFP-GEM-PTX appeared to be antagonistic for JI and synergistic for CI. As the boxplots in Fig. S4 show less bias and are less variable for the CI, the interaction was probably more synergistic, close to additivity.

In one study, synergy was described between the oncolytic adenovirus AdNuPARmE1A that target the Notch signaling pathway, in combination with gemcitabine and nab-paclitaxel in xenograft and PDX models. TFP acts on the Notch pathway via its effect on cancer stem cell marker CD44. Moreover, the authors explained that gemcitabine and paclitaxel could act together via the activation of NF-κB and trapping of the NF-κB transcription factor in order to act as a decoy system, preventing the activation of pro-survival genes and promoting apoptosis. These mechanisms of action could explain the synergy observed between TFP, GEM, and PTX because it would be an interaction between the two pathways: Notch and NF-κB. However, this adenovirus was also synergistic with gemcitabine and nab-paclitaxel used as single agents contrary to our study that showed synergy, close to additivity, of TFP with GEM and antagonism for TFP-PTX (50).

In another study, the combination of GEM with a Notch inhibitor, PF-03084014 (a selective γ-secretase inhibitor) prevented the activation of Notch target genes, inhibited tumor cell proliferation, reduced angiogenesis, decreased the tumor-resident CSC, and induced apoptosis (51).

Moreover, the synergy, close to additivity, observed can be the consequence of an interaction on the Bax/Bcl2 apoptotic pathway because, as described above, in the treatment schedule where PTX was followed by GEM, the ratio of Bax/Bcl2 increased (5). TFP is also known to increase Bax and decrease Bcl2 (8,9).

To optimize any effects further, sequential treatments should be studied. One report showed that doxorubicin (4 h) followed by PTX (24 h) and then by 48 h washout before 24 h of GEM treatment achieved the maximum effect due to cell cycle perturbations (52).

Figure 5 provides a unique "heat-spot" method for presenting a four-dimensional relationship. The graph displays the three-drug concentrations used and the colors indicate the nature of the interactions that were found. It is very complicated designing interaction studies with three drugs and concise presentation of study results can be challenging.

### Limitations

The determination of $IC_{50}$ is subject to variation depending on the plates used and on delays between the seeding and the determination of $IC_{50}$. These variations can also be due to the different methods used (MTT, sulforhodamine assay, Coulter counter) and may be the consequence of different methods of analysis (different software and equations).

The definitions and the assumptions for each interaction equation are different, but both worked well for this preliminary screening. They indicate the uncertainty of assuming simple relationships and interactions when data are limited and mechanisms are complicated. To have a better understanding of the type of interaction between these drugs and to correct any inconsistencies, a more mechanistic model is needed. Additional experiments assessing the cell cycle, apoptosis, and stem cells will provide more information for future models allowing more specificity where the interactions take place and the type of interactions (21,53).

We also assessed equations for uncompetitive and non-competitive mechanisms but they did not work. Our $\psi$ estimates exhibited very narrow confidence intervals leaving little room or need for additional interaction terms. An extension of the Ariens et al.'s (12) competitive interaction model was recently proposed (54) with addition of several interaction terms for multiple drugs similar to our $\psi$ term. Like our approach, it maybe useful for screening cell culture data prior to generating more mechanistic insights from additional measurements.

Due to the heterogeneity of CSC (31,36), it is possible that the use of one drug against one or several specific pathways will not be sufficient to affect all of the CSC; multiple drugs that are complementary to each other may be necessary.

This study was conducted *in vitro* and the nature of the interaction can change *in vivo*. For example, interaction between sorafenib and everolimus was found slightly antagonistic in cell cultures, but an *in vivo* study with mice showed a synergistic effect (55). Thus, *in vivo* xenograft experiments could confirm or disprove the degree and nature of the interactions. Use of 3-D cell cultures may offer reliability, because drug resistance found *in vivo* appeared also in 3-D cell culture for colon cancer HCT-116 cells (56,57). Moreover, a 3-D cell culture allows heterogeneity of cells combining PDAC (pancreatic ductal adenocarcinoma) and PSC. The PSC cells produce a dense extracellular matrix as well as enzymes; thus, stroma was created naturally and produced an environment closer to human tumors. The authors used methylcellulose to induce the formation of spheroids (58). These spheroids were supposed to have cancer stem-like properties. It would be interesting to study sequential treatments, as the gemcitabine-paclitaxel interaction is schedule-dependent (5).

## CONCLUSIONS

The CI and JI interaction equations do not always agree, but use of $\psi$ allows assessment of further interactions for two or three drugs. According to estimates of $\psi$, the combination of TFP-GEM was synergistic, close to additivity, and TFP-PTX was antagonistic. The interaction GEM-PTX was additive, and TFP-GEM-PTX was synergistic, close to additive. The TFP $IC_{60}$-GEM $IC_{60}$-PTX $IC_{60}$ appeared as the best combination and also reduced the number of cells by 82.1–90.2%. These results indicate reasonable potential for therapeutic benefit for this three-drug combination. Assessing the impact of each drug on CSC, cell cycling and the apoptosis pathway is needed to confirm our assumptions and provide better understanding of mechanisms of action of this three-drug combination.

## ACKNOWLEDGMENTS

This work was supported by Grant GM 24211 from the National Institutes of Health. We thank Dr. David D'Argenio for his help with ADAPT and Dr Gilbert Koch for advice on drug interaction modeling.

## NOTE

Graphs allowing rotation of Figures 2 to 5 can be found in the Supplementary Materials.

## REFERENCES

1. Cancer.net. Pancreatic cancer: treatment options: ASCO (American Society of Clinical Oncology); [updated 12/2016; cited 2017 6/6]. Available from: http://www.cancer.net/cancer-types/pancreatic-cancer/treatment-options.
2. ANSM. Summary of product characteristics (Gemcitabine): Agence nationale de sécurité du médicament et des produits de santé; [updated 29/11/2013; cited 2017 16 june]. Available from: http://agence-prd.ansm.sante.fr/php/ecodex/rcp/R0233325.htm.
3. Cancer.gov. Combination of Nab-paclitaxel and gemcitabine improves survival in patients with metastatic pancreatic cancer: National Cancer Institute; [updated 15/11/13; cited 2017 07/06]. Available from: https://www.cancer.gov/types/pancreatic/research/nab-paclitaxel-gemcitabine.
4. EMA. Summary of product characteristics (Nab-paclitaxel): European Medicine Agency; [cited 2017 16 june]. Available from: http://www.ema.europa.eu/docs/en_GB/document_library/EPAR_-_Product_Information/human/000778/WC500020435.pdf.
5. Oliveras-Ferraros C, Vazquez-Martin A, Colomer R, De Llorens R, Brunet J, Menendez JA. Sequence-dependent synergism and antagonism between paclitaxel and gemcitabine in breast cancer cells: the importance of scheduling. Int J Oncol. 2008;32(1):113–20.

6. Shu CH, Yang WK, Shih YL, Kuo ML, Huang TS. Cell cycle G2/M arrest and activation of cyclin-dependent kinases associated with low-dose paclitaxel-induced sub-G1 apoptosis. Apoptosis. 1997;2(5):463–70.
7. Polischouk AG, Holgersson A, Zong D, Stenerlöw B, Karlsson HL, Möller L, et al. The antipsychotic drug trifluoperazine inhibits DNA repair and sensitizes non-small cell lung carcinoma cells to DNA double-strand break–induced cell death. Mol Cancer Ther. 2007;6(8):2303–9.
8. Yuan K, Yong S, Xu F, Zhou T, McDonald JM, Chen Y. Calmodulin antagonists promote TRA-8 therapy of resistant pancreatic cancer. Oncotarget. 2015;6(28):25308–19.
9. Yeh C-T, Wu ATH, Chang PMH, Chen K-Y, Yang C-N, Yang S-C, et al. Trifluoperazine, an antipsychotic agent, inhibits cancer stem cell growth and overcomes drug resistance of lung cancer. Am J Respir Crit Care Med. 2012;186(11):1180–8.
10. Cheng H, Lin C-F, Shih J-H, Wu ACH, inventors; Acenda Pharma, Inc, assignee. Phenothiazine derivatives and methods of use thereof. United States patent US 9695138B1. 2017/07/04.
11. Koch G, Schropp J, Jusko WJ. Assessment of non-linear combination effect terms for drug-drug interactions. J Pharmacokinet Pharmacodyn. 2016;43(5):461–79.
12. Ariens EJ, Van Rossum JM, Simonis AM. Affinity, intrinsic activity and drug interactions. Pharmacol Rev. 1957;9(2):218–36.
13. Earp J, Krzyzanski W, Chakraborty A, Zamacona MK, Jusko WJ. Assessment of drug interactions relevant to pharmacodynamic indirect response models. J Pharmacokinet Pharmacodyn. 2004;31(5):345–80.
14. Chakraborty A, Jusko WJ. Pharmacodynamic interaction of recombinant human interleukin-10 and prednisolone using in vitro whole blood lymphocyte proliferation. J Pharm Sci. 2002;91(5):1334–42.
15. D'Argenio DZ, Schumitzky A, Wang X. ADAPT 5 user's guide: pharmacokinetic/pharmacodynamic systems analysis software. Los Angeles: Biomedical Simulations Resource; 2009.
16. Zhao L, Au JLS, Wientjes MG. Comparison of methods for evaluating drug-drug interaction. Front Biosci Elite Ed. 2010;2:241–9.
17. Yao, J, Cai H-h, Wei J-s, An Y, Ji Z-l, Lu Z-p, et al. Side population in the pancreatic cancer cell lines SW1990 and CFPAC-1 is enriched with cancer stem-like cells. Oncol Rep. 2010;23(5):1375–82.
18. Hait WN, Pierson NR. Comparison of the efficacy of a phenothiazine and a bisquinaldinium calmodulin antagonist against multidrug-resistant P388 cell lines. Cancer Res. 1990;50(4):1165–9.
19. Midha KK, Korchinski ED, Verbeeck RK, Roscoe RMH, Hawes EM, Cooper JK, et al. Kinetics of oral trifluoperazine disposition in man. Br J Clin Pharmacol. 1983;15(3):380–2.
20. Verbeeck RK, Cardinal J-A, Hill AG, Midha KK. Binding of phenothiazine neuroleptics to plasma proteins. Biochem Pharmacol. 1983;32(17):2565–70.
21. Zhu X, Straubinger RM, Jusko WJ. Mechanism-based mathematical modeling of combined gemcitabine and birinapant in pancreatic cancer cells. J Pharmacokinet Pharmacodyn. 2015;42(5):477–96.
22. Avan A, Crea F, Paolicchi E, Funel N, Galvani E, Marquez VE, et al. Molecular mechanisms involved in the synergistic interaction of the EZH2 inhibitor 3-deazaneplanocin A with gemcitabine in pancreatic cancer cells. Mol Cancer Ther. 2012;11(8):1735–46.
23. Kroep JR, Giaccone G, Voorn DA, Smit EF, Beijnen JH, Rosing H, et al. Gemcitabine and paclitaxel: pharmacokinetic and pharmacodynamic interactions in patients with non-small-cell lung cancer. J Clin Oncol. 1999;17(7):2190–7.
24. Yilmaz B, Kadioglu YY, Aksoy Y. Investigation of the pharmacokinetics of gemcitabine and 2′,2′-difluorodeoxyuridine in human plasma by liquid chromatography. Anal Biochem. 2004;332(2):234–7.
25. Administration FaD. Gemcitabine injection [updated 8/2017 cited 2017 10/23]. Available from: https://www.accessdata.fda.gov/drugsatfda_docs/label/2017/209604s000lbl.pdf.
26. Esumi Y, Mitsugi K, Seki H, Takao A, Kawai M. Placental transfer, lacteal transfer and plasma protein binding of gemcitabine. Xenobiotica. 1994;24(10):957–64.
27. Liebmann JE, Cook JA, Lipschultz C, Teague D, Fisher J, Mitchell JB. Cytotoxic studies of paclitaxel (Taxol®) in human tumour cell lines. Br J Cancer. 1993;68(6):1104–9.
28. Administration FaD. Clinical pharmacology and biopharmaceutics review 2004 [updated 2004; cited 2017 10/23]. Available from: https://www.accessdata.fda.gov/drugsatfda_docs/nda/2005/21660_ABRAXANE_biopharmr.PDF.
29. Administration FaD. ABRAXANE for injectable suspension (paclitaxel protein-bound particles for injectable suspension) (albumin-bound) [updated 01/07/2005; cited 2017 10/23]. Available from: https://www.accessdata.fda.gov/drugsatfda_docs/label/2005/021660lbl.pdf.
30. Skoda J, Hermanova M, Loja T, Nemec P, Neradil J, Karasek P, et al. Co-expression of cancer stem cell markers corresponds to a pro-tumorigenic expression profile in pancreatic adenocarcinoma. PLoS One. 2016;11(7):1–18.
31. Penchev VR, Rasheed ZA, Maitra A, Matsui W. Heterogeneity and targeting of pancreatic cancer stem cells. Clin Cancer Res. 2012;18(16):4277–84.
32. Lee G, Hall RR, Ahmed AU. Cancer stem cells: cellular plasticity, niche, and its clinical relevance. J Stem Cell Res Ther. 2016;06(10):1–20.
33. Breidert M, Keck T, Makowiec F, Lohrmann C, Harder J, Fischer R. Early recurrence of pancreatic cancer after resection and during adjuvant chemotherapy. Saudi J Gastroenterol. 2012;18(2):118–21.
34. Lonardo E, Cioffi M, Sancho P, Crusz S, Heeschen C. Studying pancreatic cancer stem cell characteristics for developing dew treatment strategies. J Vis Exp. 2015;100:1–9.
35. Vaz AP, Ponnusamy MP, Seshacharyulu P, Batra SK. A concise review on the current understanding of pancreatic cancer stem cells. J Cancer Stem Cell Res. 2014;2(4):1–12.
36. Rao CV, Mohammed A. New insights into pancreatic cancer stem cells. World J Stem Cells. 2015;7(3):547–55.
37. Zhu Y-Y, Yuan Z. Pancreatic cancer stem cells. Am J Cancer Res. 2015;5(3):894–906.
38. Rajeshkumar NV, Rasheed ZA, Garcia-Garcia E, Lopez-Rios F, Fujiwara K, Matsui WH, et al. A combination of DR5 agonistic monoclonal antibody with gemcitabine targets pancreatic cancer stem cells and results in long-term disease control in human pancreatic cancer model. Mol Cancer Ther. 2010;9(9):2582–92.
39. Li C, Wu JJ, Hynes M, Dosch J, Sarkar B, Welling TH, et al. c-Met is a marker of pancreatic cancer stem cells and therapeutic target. Gastroenterology. 2011;141(6):2218–27. e5
40. Kroep J, Giaccone G, Tolis C, Voorn D, Loves W, Van Groeningen C, et al. Sequence dependent effect of paclitaxel on gemcitabine metabolism in relation to cell cycle and cytotoxicity in non-small-cell lung cancer cell lines. Br J Cancer. 2000;83(8):1069–76.
41. Frese KK, Neesse A, Cook N, Bapiro TE, Lolkema MP, Jodrell DI, et al. nab-Paclitaxel potentiates gemcitabine activity by reducing cytidine deaminase levels in a mouse model of pancreatic cancer. Cancer Discov. 2012;2(3):260–9.
42. Shord SS, Patel SR. Paclitaxel alters the expression and specific activity of deoxycytidine kinase and cytidine deaminase in non-small cell lung cancer cell lines. J Exp Clin Cancer Res. 2009;28:76.
43. Shord SS, Camp JR, Young L. Paclitaxel decreases the accumulation of gemcitabine and its metabolites in human leukemia cells and primary cell cultures. Anticancer Res. 2005;25(6B):4165–72.
44. Shord SS, Faucette SR, Gillenwater HH, Pescatore SL, Hawke RL, Socinski MA, et al. Gemcitabine pharmacokinetics and interaction with paclitaxel in patients with advanced non-small-cell lung cancer. Cancer Chemother Pharmacol. 2003;51(4):328–36.
45. Theodossiou C, Cook JA, Fisher J, Teague D, Liebmann JE, Russo A, et al. Interaction of gemcitabine with paclitaxel and cisplatin in human tumor cell lines. Int J Oncol. 1998;12(4):825–32.

46. Porter C, Waddell JA, Solimando JD. Cancer chemotherapy update: nab-paclitaxel plus gemcitabine regimen for pancreatic cancer. Hosp Pharm. 2014;49(1):18–22.
47. Von Hoff DD, Ervin T, Arena FP, Chiorean EG, Infante J, Moore M, et al. Increased survival in pancreatic cancer with nab-paclitaxel plus gemcitabine. N Engl J Med. 2013;369(18):1691–703.
48. Lee JH, Kim SK, Khawar IA, Jeong SY, Chung S, Kuh HJ. Microfluidic co-culture of pancreatic tumor spheroids with stellate cells as a novel 3D model for investigation of stroma-mediated cell motility and drug resistance. J Exp Clin Cancer Res. 2018;37(1):4.
49. Meng H, Wang M, Liu H, Liu X, Situ A, Wu B, et al. Use of a lipid-coated mesoporous silica nanoparticle platform for synergistic gemcitabine and paclitaxel delivery to human pancreatic cancer in mice. ACS Nano. 2015;9(4):3540–57.
50. Mato-Berciano A, Raimondi G, Maliandi MV, Alemany R, Montoliu L, Fillat C. A NOTCH-sensitive uPAR-regulated oncolytic adenovirus effectively suppresses pancreatic tumor growth and triggers synergistic anticancer effects with gemcitabine and nab-paclitaxel. Oncotarget. 2017;8(14):22700–15.
51. Yabuuchi S, Pai SG, Campbell NR, de Wilde RF, De Oliveira E, Korangath P, et al. Notch signaling pathway targeted therapy suppresses tumor progression and metastatic spread in pancreatic cancer. Cancer Lett. 2013;335(1):41–51.
52. Zoli W, Ricotti L, Barzanti F, Dal Susino M, Frassineti GL, Milandri C, et al. Schedule-dependent interaction of doxorubicin, paclitaxel and gemcitabine in human breast cancer cell lines. Int J Cancer. 1999;80(3):413–6.
53. Miao X, Koch G, Straubinger RM, Jusko WJ. Pharmacodynamic modeling of combined chemotherapeutic effects predicts synergistic activity of gemcitabine and trabectedin in pancreatic cancer cells. Cancer Chemother Pharmacol. 2016;77(1):181–93.
54. Wicha SG, Chen C, Clewe O, Simonsson USH. A general pharmacodynamic interaction model identifies perpetrators and victims in drug interactions. Nat Commun. 2017;8(1):2129.
55. Pawaskar DK, Straubinger RM, Fetterly GJ, Hylander BH, Repasky EA, Ma WW, Jusko WJ. Synergistic interactions between sorafenib and everolimus in pancreatic cancer xenografts in mice. Cancer Chemother Pharmacol. 2013;71(5):1231–40.
56. Karlsson H, Fryknas M, Larsson R, Nygren P. Loss of cancer drug activity in colon cancer HCT-116 cells during spheroid formation in a new 3-D spheroid cell culture system. Exp Cell Res. 2012;318(13):1577–85.
57. Temraz S, Mukherji D, Alameddine R, Shamseddine A. Methods of overcoming treatment resistance in colorectal cancer. Crit Rev Oncol Hematol. 2014;89(2):217–30.
58. Ware MJ, Keshishian V, Law JJ, Ho JC, Favela CA, Rees P, et al. Generation of an in vitro 3D PDAC stroma rich spheroid model. Biomaterials. 2016;108:129–42.